AIP Advances

Photoluminescence excitation spectroscopy for structural and electronic characterization of resonant tunneling diodes for THz applications

Cite as: AIP Advances **11**, 035122 (2021); https://doi.org/10.1063/5.0035394
Submitted: 02 February 2021 . Accepted: 18 February 2021 . Published Online: 08 March 2021

M. Cito, O. Kojima, B. J. Stevens, T. Mukai, and R. A. Hogg

Photoluminescence excitation spectroscopy for structural and electronic characterization of resonant tunneling diodes for THz applications

Cite as: AIP Advances 11, 035122 (2021); doi: 10.1063/5.0035394
Submitted: 2 February 2021 • Accepted: 18 February 2021 •
Published Online: 8 March 2021

M. Cito,[1,a] O. Kojima,[2] B. J. Stevens,[3] T. Mukai,[4] and R. A. Hogg[1]

AFFILIATIONS

[1] School of Engineering, University of Glasgow, Oakfield Avenue, G12 8LT Glasgow, United Kingdom
[2] Department of Electrical and Electronic Engineering, Kobe University, Kobe 657-8501, Japan
[3] EPSRC National Centre for III-V Technologies, Department of Electronic & Electrical Engineering, University of Sheffield, North Campus, Broad Lane, Sheffield S37HQ, United Kingdom
[4] Sensing Technology R & D Project, R & D Headquarters, RohmCo.Ltd., 21 Saiin Mizosaki-cho, Ukyo-ku, Kyoto 615-8585, Japan

[a] **Author to whom correspondence should be addressed:** michele.cito@glasgow.ac.uk

ABSTRACT

Photoluminescence excitation spectroscopy (PLE) and high-resolution x-ray diffraction (HR-XRD) are used to characterize the structural and electronic properties of high current density InGaAs/AlAs/InP resonant tunneling diode wafer structures. The non-destructive assessment of these structures is challenging, with several unknowns: well and barrier thickness, the well indium molar fraction, and band-offsets, which are a function of strain, material, growth sequence, etc. The low temperature PL spectra are deconvoluted through simulation and are shown to include contributions from type I (e1–hh1) and type II (conduction band–hh1) transitions that are broadened due to interface fluctuations on a range of length scales. PLE data are obtained by a careful choice of the detection wavelength, allowing the identification of the e2hh2 transition that is critical in determining the band-offsets. An agreement between the HR-XRD data, the PL, and the PLE data is only obtained for a given conduction band offset of 58.8%. This scheme, combining HR-XRD, PL, and PLE, consequently provides crucial electronic and structural information non-destructively.

Wireless data-demand has increased tremendously in the last decade,[1] and there is now market demand for efficient, compact, low cost sources covering the THz spectrum (0.1 THz–10 THz).[2] This range of frequencies is still referred to as the terahertz gap, positioned between microwave and optical technologies. The development of THz emitters is a highly active field, and resonant tunneling diodes (RTDs) have emerged as a strong candidate to service the THz gap, with fundamental oscillations as high as 1.98 THz being demonstrated,[3] remaining the highest frequency semiconductor oscillator. Devices operate at room temperature, with good tunability and compact dimensions, in line with the market requirements.

RTD structures are generally realized using a thin quantum well (QW) (~4 nm) to reduce the electron transit time, and for high current density designs, the QW is even thinner (2.5 nm–4 nm).[4] RTD epitaxy has been performed using both molecular beam epitaxy (MBE)[5] and metalorganic vapor-phase epitaxy (MOVPE)[6] reactors, but despite the outstanding precision of these techniques, the characterization processes present a range of issues leading, in turn, to difficulties in optimization of the epitaxial processes. The use of a single QW makes x-ray diffraction less informative than in the case of a multi-layer stack,[7] and room temperature photoluminescence (PL) of the highly doped structure may be uninformative.[8] Non-destructive wafer characterization provides critical information on structural and electrical properties and is also fundamental for the reproducibility of the growth process and hence device engineering and commercialization.

To improve the reproducibility and the mass-manufacture of low-cost tunnel devices, we previously showed that low temperature PL spectroscopy provided a fast characterization technique,[9]

and its combination with high-resolution x-ray diffraction (HR-XRD) and the inclusion of a buried undoped "copy" QW provided a robust non-destructive characterization scheme.[7] PL also proved to be a powerful spectroscopy technique in analyzing RTD electron charge build-up in the QW.[10] Standard band-offsets were assumed,[11] but these are known to be dependent on the local strain vectors caused by the lattice mismatch, resulting in a range of possible values depending on the semiconductor alloys involved in the heterointerfaces.[12]

In this paper, we apply low temperature photo-luminescence excitation (PLE) spectroscopy to RTD epitaxial wafer characterization. In combination with room temperature HR-XRD, line-shape fitting of the low temperature PL spectrum, and simulation, the observation of higher order optical transitions allows us to unambiguously determine the band-offsets and all key structural parameters of the RTD. This method has significant speed and resource advantages over methods that require fabrication and testing of a family of RTD wafers.[13] Furthermore, this technique allows the non-destructive determination and verification of the band-structure and the energy level profile of the device, providing additional information critical to device engineering and reproducible manufacturing. A conduction band offset of 58% is obtained for these structures, and the origin of this lower than expected value is discussed.

The InP/InGaAs/AlAs RTD structures described here were grown in a vertical Thomas close-coupled shower head MOVPE reactor on (100) semi-insulating InP:Fe substrates. Details about the growth process are reported elsewhere.[14] The sequence of epitaxy for the RTD structure consists of a 100 nm InP buffer layer followed by 200 nm $In_{0.53}Ga_{0.47}As$ and 400 nm highly n-doped $In_{0.53}Ga_{0.47}As$ (2×10^{19} cm^{-3} Si) as the lower contact. A 20 nm n-doped $In_{0.53}Ga_{0.47}As$ (3×10^{18} cm^{-3} Si) emitter layer is then grown, followed by a 2 nm $In_{0.53}Ga_{0.47}As$ spacer layer. An $In_{0.85}Ga_{0.20}As$ quantum well is formed between two 1.1 nm AlAs barriers. On the collector side, a 20 nm $In_{0.53}Ga_{0.47}As$ spacer layer is grown with a 25 nm $In_{0.53}Ga_{0.47}As$ (3×1018 cm^{-3} Si) collector layer. The epitaxy is terminated with 15 nm n-doped $In_{0.53}Ga_{0.47}As$ (2×10^{19} cm^{-3} Si) and 8 nm $In_{0.80}Ga_{0.20}As$ (2×10^{19} cm^{-3} Si) to improve the conductivity at the collector side.

The characterization process is focused on four main variables, the barrier thickness B_{th}, the well thickness W_{th}, the indium molar fraction of the QW [In %], and the band offset ratio Q. The indium fraction for the nominally lattice matched layers can be readily determined by HR-XRD. The structural parameters are expressed in units of one mono-layer (1 ML = $a_{InP}/2 \approx 0.293$ nm). HR-XRD was performed using a Philips Analytical X'Pert PRO.[7]

Figure 1 shows the experimental HR-XRD data (green) and an optimal data fit (light green, shifted to a lower position to help the reader). From the fitting, we extrapolated the physical parameters, finding bulk LM-InGaAs on InP (the main peak at 31.517°, offset included) and slightly lattice-mismatched InAlAs (lower peak at 31.46°). For the QW, we deduced a well thickness of $W_{th} = 4.3 \pm 0.7$ nm (15 ± 2 MLs), [In] = 83.5 ± 7%, and a barrier thickness of $B_{th} = 1.1$ nm (4 MLs). Data fitting is obtained using linked-epitaxial layers (identical alloys have the same composition and growth rates), and these results are in line with the range of errors indicated by TEM imaging of these samples.[7]

The two insets in Fig. 1 show the error introduced by a ±1 ML fluctuation in the barrier thickness. Inset A, focused on the In-rich

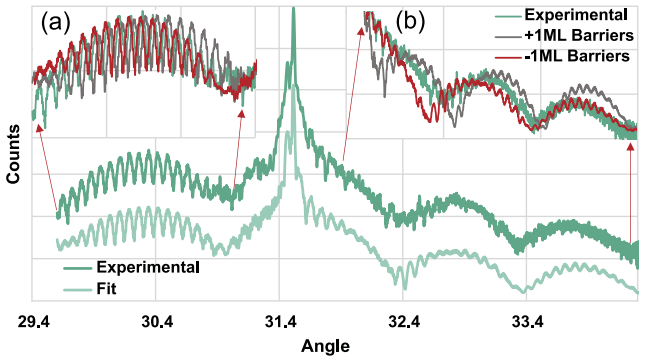

FIG. 1. HR-XRD experimental data (green) and fitting (light green). Insets A and B show the effect of 1 ML fluctuation on the barrier thickness (−1 ML in red and +1 ML in gray, both simulated) compared with the experimental data (green).

QW region, shows that the curves are not perfectly overlapped, indicating the very poor fit for these conditions. Inset B, focused on the tensile region of the graph that directly involves the AlAs barrier, further indicates the disagreement of these simulation conditions with the experiment. We, therefore, consider the variation in barrier thickness to be no more than ±0.5 ML.[7]

One may consider the introduction of an MQW layer below the RTD structure to assist in structural characterization. However, the QW and barriers are highly strained, and an MQW risks strain relaxation and the introduction of deleterious effects to the RTD operation. We note that a single "copy" undoped QW below the active device can provide improvements in HR-XRD signal to noise[7] and allow unambiguous determination of type I and type II PL signals.[8]

Figure 2 shows a schematic representation of the low-temperature conduction and valence band profile of the QW, key electron and hole states, and observable radiative emissions. Band line-ups were obtained based on the model-solid theory.[11]

Simulation were developed in NextNano,[15] first solving the strain equations and then correcting the band line-ups including the asymmetric doping profile (emitter and collector), the spacers, and the highly doped In-rich contact cap. On this basis, the Schrödinger–Poisson equations are solved self-consistently on the QW region. QW ternary compound effective masses are calculated by software considering the temperature and the strain conditions, with parameters from the work by Vurgaftman *et al.*[16]

The black vertical axis shows key energy values (e.g., bound states and barrier height). The E = 0 eV point is set at the bulk LM-InGaAs conduction band potential. Type I transitions are defined for transitions between spatially coincident confined energy states in the conduction and valence band. Type II transitions are generated by the recombination of holes in the QW with electrons in the bulk LM-InGaAs material. The n = 1 electron–heavy hole (e1–hh1) type I transition, the type II transition, and the bulk transitions are detected by PL (solid line).[17]

Figure 3(a) plots the type I transition energy (e1–hh1) as a function of QW indium molar fraction and QW thickness, utilizing band offsets of 65%. The effect of QW thickness on the PL transition energy is highlighted, with a variation of 0.13 meV for a QW thickness of 11 ML–16 ML with ~2 meV variation for 1 ML change in

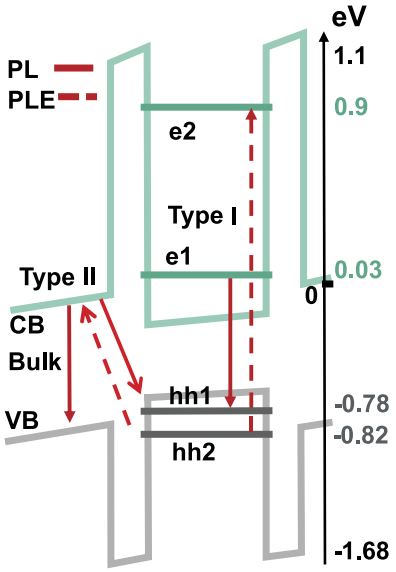

FIG. 2. Schematic representation of the RTD active region band profile; horizontal lines indicate the confined electron(dark green) and heavy hole states(dark gray). Vertical arrows indicate the radiative emission detectable by PL (solid lines) and PLE (dashed lines). Energy references are reported through the black vertical arrow on the right side, and the origin is positioned on the bulk conduction band.

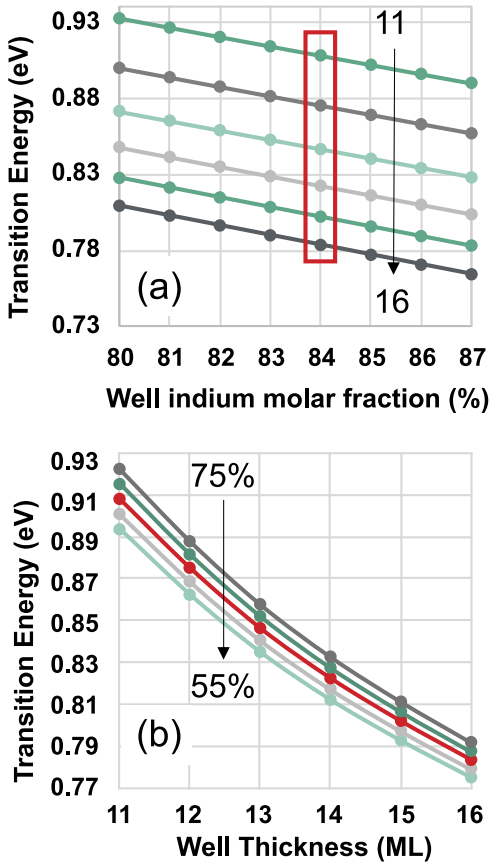

FIG. 3. (a) Simulation-based type I transition sensitivity analysis and (b) energy change varying the band offset.

QW width. The red box highlights the calculated transition energies for a range of QW thicknesses for a given indium composition. Figure 3(b) plots the variation in calculated transition energies of these possible structures as a function of varying band-offset from 75% to 55% at steps of 5%. A ±10% variation in band-offsets is within the scatter we see in the literature.[12] All simulations are computed assuming a barrier thickness of 4.0, in line with XRD fitting of structural parameters that yield barrier widths of 4.0 ± 0.5 ML. Simulation of the effect of these changes in barrier width on the electronic structure indicate a ~1 meV variation in transition energies. Based on this analysis, we are able to reduce the number of system variables from 4 to 3 as the variation in barrier width is removed.

Figure 4 (black line) plots the 4 K photoluminescence spectrum of the sample obtained with 1 mW/cm^2 excitation at 915 nm. The comparatively sharp central peak at 0.801 eV is attributed to the bulk LM-InGaAs transition. For lower energy, the broad peak at 0.78 eV is associated with the type II transition (see Fig. 2), while the spectrum is more complicated for higher energy. LM-InGaAs is n-doped, resulting in bandgap renormalization and band-filling effects that result in a main peak (zone center) and higher energy transitions.[8] In addition, we expect a type I PL signal from the QW. We observe two broad peaks (0.812 eV and 0.838 eV) tentatively associated with the type I QW emission. We, therefore, wish to deconvolve the spectrum to understand the origin of the radiative transitions.

The growth process of a QW suffers from fluctuations in the well thickness and roughness of the interfaces, causing broadening of the optical transitions. The impact of these depends upon their magnitudes and length-scales.[18] Previous structural studies[17] and the form of the PL spectrum[19] suggest that large-scale monolayer fluctuations of well width (i.e., greater than the exciton radius) and small scale monolayer fluctuations are at play.[7]

Our deconvolution is obtained using 3 Gaussian peaks (μ, σ_{T1}) for the type I transition (X ML, ±1 ML), and their positions on the energy axis (μ) are determined by the simulation described in Fig. 3 and are based on several constraints. Inspection of Fig. 3 indicates essentially identical energy splitting between transitions for ±1 ML well width fluctuations. We, therefore, introduce this rule in assigning peak positions to the fit. The increase in energy splitting of the transitions with decreasing well width places a limit on possible well-widths (X) for the structure. Based on the essentially equal splitting of the transitions, we assume an equal linewidth (σ_{T1}) for the three type I transitions.

For the type II transitions, we adopt a similar process, with 3 Gaussian peaks (μ, σ_{T2}) for the type I transition (X ML, ±1 ML). Here, the energetic position is again dictated by simulation, with the linewidths (σ_{T2}) governed by only variation in the hole transition energies. The ratio of integrated intensity of the X, +1 ML, and −1 ML transitions for the type I and type II transitions is kept constant. The ratio of the type I to type II emission (T1/T2) is a fit parameter.

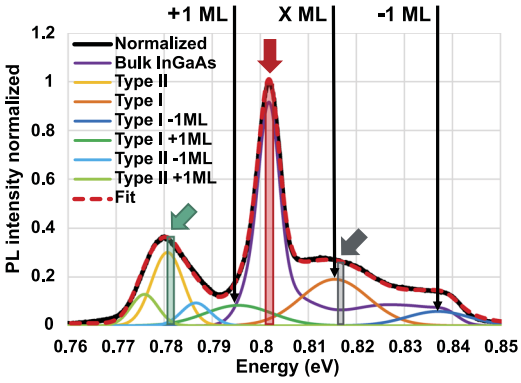

FIG. 4. Experimental PL spectra (black line) and fitted spectra (red dashed line). Black lines highlight the ΔE between adjacent ML solution (+1/X and X/−1). Thick arrows and squares indicate the chosen PLE detection energies at ~0.781 eV (green) and ~0.81 eV (red).

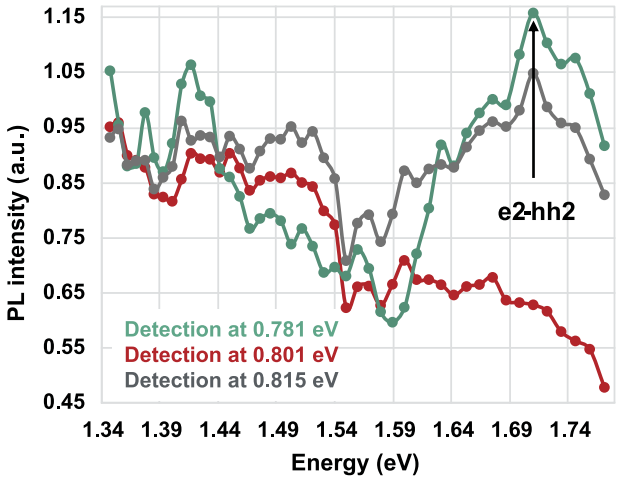

FIG. 5. PLE spectra detected at 0.781 eV (green) and on the lattice match bulk InGaAs at 0.801 eV (red). The black line indicates the resonance peak at 1.71 eV attributed to the e2–hh2 transition.

The red line in Fig. 4 is our fit to the spectrum utilizing σ_{T1} = 7 meV and σ_{T2} = 3 meV and T2/T1 = 1.57 ± 0.01 utilizing band-offsets of 59%. An excellent fit is obtained. As a result of the fit, we can observe that the 0.78 eV feature is the sum of the 3 type II peaks, at 0.775 eV, 0.781 eV, and 0.786 eV. The linewidth of the LM-InGaAs is deduced through deconvolution due to overlap with the +1 ML and XML transitions and is 4 meV, which is in line with the limit of 3.3 meV at 0 K predicted for perfect LM-InGaAs.[20] The higher energy features are more complex, made up of intra-band momentum conserving transitions indicated as X and −1 ML QW emission at 0.815 eV and 0.839 eV, respectively.

The PLE measurements were also performed at 4 K by taking PL spectra at the same power density but tuning the excitation wavelength (a Ti:sapphire laser) from 920 nm to 700 nm in 5 nm steps. Once the data are acquired, suitable wavelength "energy bins" of the PL spectrum are selected to allow the PLE spectrum to be plotted. In order to provide unambiguous results, specific regions are selected in Fig. 4. The green arrow indicates the region between 0.781 eV and 0.782 eV, corresponding to the X ML type II transition. This is chosen to minimize overlap with other spectral features; on the low energy side, this is from the +1 ML type II peak (green curve) while on the high energy side, there is contribution from both the −1 ML type II (blue curve) and the +1 ML type I peaks (dark green curve). This is covered in more detail in supplementary material S1. Another isolated feature is marked with the red arrow (0.801 eV–0.802 eV) corresponding predominantly to the bulk LM-InGaAs transition. The final PLE detection range discussed is marked by the gray arrow (0.815 eV–0.816 eV) on the XML type I peak. Here, there is a strong contribution to the PL signal from the highly doped LM-InGaAs material.

Figure 5 plots the PLE spectrum obtained in these three cases plotted in green, red, and gray, respectively. As the excitation wavelength is reduced, the penetration depth can be expected to reduce. For the LM-InGaAs transition, this results in a gradual decrease in signal intensity with increasing excitation energy. For the X ML type II transition, we observe a clear resonance at 1.71 eV with a linewidth of ~50 meV that is attributed to the type I e2–hh2 transition. Considering the linewidth of the type I PL transition being ~14 meV (ΔE/E = 0.017), double this value can be expected for the e2–hh2 transition (0.058), in good agreement with observation. The feature at 1.71 eV is less pronounced when we move the PLE detection range to the peak of the XML type I emission. This is attributed to the strong contribution of LM-InGaAs PL at this detection wavelength, making this PLE trace the convolution of the other two PLE traces that have a comparatively "purer" origin to their PL signals.

The feature at ~1.42 eV has an energy close to e1–hh4 type I (~1.44 eV) and conduction band–hh4 type II (~1.40 eV), both for the −1 ML solution. Due to the peaks overlapping in the PL spectra, this emission cannot be confirmed, and it is excluded from the analysis.

With measured energies for type I e1–hh1, type I e2–hh2, and the type II transition between the bulk LM-InGaAs conduction and holes bound within the quantum well (hh1), we are now able to uniquely determine the band-offset, quantum well width, and composition. Figure 6 plots the required band-offset, indium composition, and thickness of the well to realize the observed energies for the aforementioned optical transitions. For a 14 ML quantum well, with 83.9% indium and a band-offset of 58.8%, we observe an intersection (marked with a red circle), indicating that these are the structural and electronic characteristics of our structure.[21]

The green square indicates a region where the intersection of all three lines is next closest and provides the best po1ssible candidate to confound our analysis. A fit may only be considered at this point if we have sufficient error for determining the energy of either the type I e1–hh1 or type II PL transition. Inspecting Fig. 6, this would be sufficient error to be unable to detect a change of ~2% points in indium composition. Cross referencing back to Fig. 3(a), this corresponds to a required error in peak assignment for the type I e1–hh1 transition of ~10 meV–15 meV. Inspection of Fig. 4 indicates that this appears highly unlikely, and we are unable to use these parameters to provide an adequate fit to the PL spectrum.

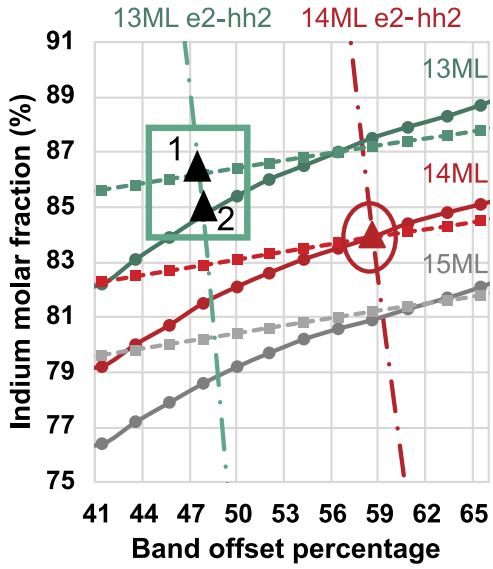

FIG. 6. Iso-energy plot of the resolved PL-PLE energies obtained experimentally: e2–hh2 = 1.71 eV (dashed-dotted lines), type I = 0.815 eV (solid lines), and type II = 0.781 eV (dashed lines with squares). Results are reported for 3 QW thickness solutions: 13 ML (green), 14 ML (red), and 15 ML (gray).

In summary, we have reported the non-destructive wafer characterization of AlAs/InGaAs high current density resonant tunneling diode structures using XRD, low temperature PL, and PLE. We show how simulation and deconvolution of the PL spectrum allow ideal PLE detection energy to be determined. Critically, the e2–hh2 transition detected by PLE gives an additional energy feature in the band profile, in addition to a type I e1–hh1 transition, and type II transition, allowing us to determine the conduction band offset ratio, in addition to key structural parameters: the QW width and composition.

See the supplementary material for further PLE analysis. Supplement1 provides additional information and analysis of the effect of PLE detection ranges. Supplement2 shows the methodology being applied on another sample to further demonstrate its validity.

This project has received funding from the European Union's Horizon 2020 research and innovation program under Marie Skłodowska-Curie Grant, Agreement No. 765426 (TeraApps). We are thankful for the help by Dr. Matthew Steer of the School of Engineering (UoG) with the HR-XRD apparatus.

DATA AVAILABILITY

The data that support the findings of this study are available from the corresponding author upon reasonable request.

REFERENCES

[1] S. Cherry, IEEE Spectrum **41**, 58 (2004).
[2] T. Nagatsuma, IEICE Electron. Express **8**, 1127 (2011).
[3] R. Izumi, S. Suzuki, and M. Asada, in *42nd International Conference on Infrared, Millimeter, and Terahertz Waves (IRMMW-THz)* (IEEE, 2017).
[4] H. Kanaya, H. Shibayama, R. Sogabe, S. Suzuki, and M. Asada, Appl. Phys. Express **5**, 124101 (2012).
[5] M. Feiginov, H. Kanaya, S. Suzuki, and M. Asada, Appl. Phys. Lett. **104**, 243509 (2014).
[6] H. Sugiyama, H. Yokoyama, A. Teranishi, S. Suzuki, and M. Asada, Jpn. J. Appl. Phys., Part 1 **49**, 051201 (2010).
[7] R. Baba, K. J. P. Jacobs, B. A. Harrison, B. J. Stevens, and T. Mukai, R. A. Hogg, J. Appl. Phys. **126**, 124304 (2019).
[8] K. J. Jacobs,R. Baba, B. J. Stevens, T. Mukai, R. A. Hogg, in *41st International Conference on Infrared, Millimeter, and Terahertz waves (IRMMW-THz)* (IEEE, 2016), p. 1.
[9] K. J. P. Jacobs, B. J. Stevens, and R. A. Hogg, IEICE Trans. Electron. **E99.C**, 181 (2016).
[10] M. S. Skolnick, D. G. Hayes, C. R. H. White, P. E. Simmonds, L. Eaves, A. W. Higgs, M. Henini, O. H. Hughes, G. W. smith, and C. R. Whitehouse, Phys. Scr. **T39**, 271 (1991).
[11] C. G. Van de Walle, Phys. Rev. B **39**, 1871 (1989).
[12] S. C. Jain, M. Willander, and H. Maes, Semicond. Sci. Technol. **11**, 641 (1996).
[13] K. Fobelets, R. Vounckx, J. Genoe, R. Mertens, and G. Borghs, Superlattices Microstruct. **11**, 27 (1992).
[14] K. J. P. Jacobs, B. J. Stevens, T. Mukai, D. Ohnishi, and R. A. Hogg, J. Cryst. Growth **418**, 102 (2015).
[15] S. Birner, T. Zibold, T. Andlauer, T. Kubis, M. Sabathil, A. Trellakis, and P. Vogl, IEEE Trans. Electron Devices **54**, 2137 (2007).
[16] I. Vurgaftman, J. R. Meyer, and L. R. Ram-Mohan, J. Appl. Phys. **89**, 5815 (2001).
[17] R. Baba, O. Kojima, K. J. P. Jacobs, B. A. Harrison, B. J. Stevens, T. Mukai, and R. A. Hogg, Proc. SPIE **10929**, 1092909 (2019).
[18] J. Christen, M. Grundmann, and D. Bimberg, J. Vac. Sci. Technol. B **9**, 2358 (1991).
[19] M. A. Herman, D. Bimberg, and J. Christen, J. Appl. Phys. **70**, R1 (1991).
[20] G. Landgren, J. Wallin, and S. Pellegrino, J. Electron. Mater. **21**, 105 (1992).
[21] G. Duggan, J. Vac. Sci. Technol. B **3**, 1224 (1985).